LOAD-DISPLACEMENT AND STABILITY CHARACTERISTICS OF THIN-WALLED BEAMS WITH SINGLY SYMMETRIC OR NON-SYMMETRIC CROSS-SECTIONS

Dellelegne Teshome
Civil Engineering Department
Addis Ababa University

ABSTRACT

The governing differential equations that had been derived following the finite displacement formulation and the corresponding general stiffness equations are closely scrutinized. Previous applications of the derivations were restricted to doubly- and singly-symmetric I-section beams. In the present study, the relevant terms in the above equations that take into account other cross-sectional symmetry conditions are explicitly and efficiently determined. These have been applied in several examples illustrating studies on the nonlinear lond-displacement behavior of members with arbitrary cross-sections including the mono-symmetric channel section beams which have horizontal axes of symmetry, and the non-symmetric Z-section beams. Further, the same refinements were applied to the reduced formulations which contain only lateral and torsional degrees of freedom, and these have been applied for the determination of lateral torsional buckling loads and for plotting linearized load-displacement curves. These studies showed that only the channel sections failed to exhibit any buckling phenomenon. However, all sections studied were seen to be affected by the location of the load point. The Z- and channel section beams seemed to posses large reserve strength as compared to the I- section beams. However, it was believed that this reserve strength corresponds to fairly large stresses.

INTRODUCTION

Thin-walled sectioned beams are extensively used in present day steel buildings, bridges, and other structures due to their simplicity in fabrication and construction. Such structural members combine lightness with a relatively large load carrying capacity. There are a large number of cross-sectional shapes in use in steel structures, and the simplest and the mast common of these are the I-shapes, Z-shapes, and the channels. While the I-shaped cross-section beams had received extensive coverage in experimental and theoretical research, the mono-symmetric channels and the non-symmetric Z-shaped beams seem to have largely been neglected. Further, the unsymmetrical nature of the latter two sections involves considerations not encountered in the usual I-shapes.

The finite displacement formulation is used for load-displacement and stability analysis of the mono-symmetric channel and the none-symmetric Z-section beams, and the results obtained are compared with those of the I-section beams. Due to the availability of extensive computational facilities, the computational scheme based on the finite element technique will be applied to the generalized nonlinear method as well as to the linearized method of load-displacement analysis. Both of these investigations will expose the lateral-torsional instability characteristics of the members.

THEORETICAL BACKGROUND

General Formulation

Consider a general thin-walled member which is subjected to the transverse nodal forces F_{yk} and F_{zk}, and to the distributed transverse and torsional loads p_z, p_y, and c_t, along its length, as shown in Fig.1. The axes x, y, and z form a right-handed Cartesian coordinate system, and u_c is the displacement of the centroid C along the x-axis, while v_s and w_s represent the displacements of the shear center S in the y- and z- directions, respectively. Also, ϕ represents the rotation of the cross-section about the shear center. Rigorous expressions for the displacement field u, v, and w of an arbitrary point across a section were given [5] as;

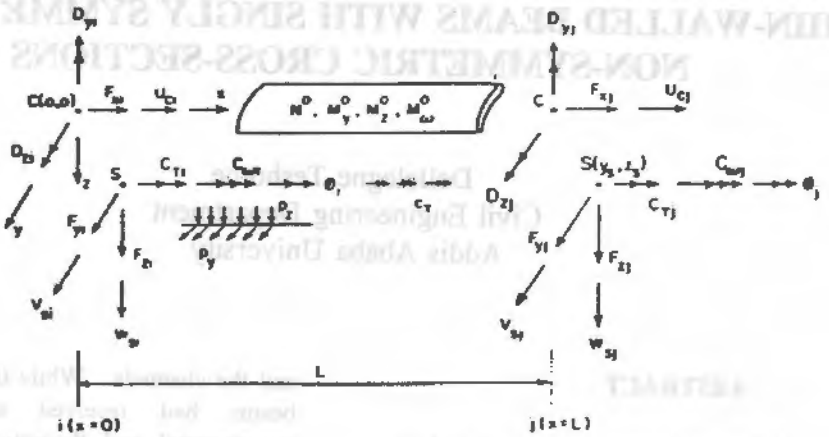

Figure 1 Element of a Thin-Walled member

$$u = u_c\text{-}(y\text{Cos}\phi\text{-}z\text{Sin}\phi)v_s'\text{-}(z\text{Cos}\phi + y\text{Sin}\phi)w_s' \quad \text{(1a)}$$

$$v = v_s\text{-}(y - y_s)(1 - \text{Cos}\phi) - (z - z_s)\text{Sin}\phi \quad \text{(1b)}$$

$$w = w_s\text{-}(y - y_s)\text{Sin}\phi - (z - z_s)(1 - \text{Cos}\phi) \quad \text{(1c)}$$

It is to be noted that all components of the displacement field of Eq. (1) are incremental quantities in the present formulation. Also, it is to be emphasized that, the transverse nodal and distributed loads may be applied at arbitrary points (y_p, z_p) and (y_s, z_p), which are on the horizontal and vertical axes containing the shear center, as shown in Fig. 2, but not exactly at the shear center.

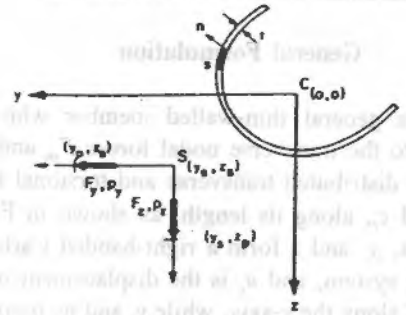

Figure 2 Load-Point Location

The general virtual work equation of such a beam element in the updated finite displacement approach, that is after neglecting the third and higher order terms, can be expressed as [5]:

$$\begin{aligned}&\int_v (\sigma_{ij}^o \delta e_{ij}^{NL} + \sigma_{ij}^L \delta e_{ij}^L) dV \\ &- \int_s (p_i^o \delta u_i^{NL} + p_i \delta u_i^L) dx \\ &- [F_{ik}^o \delta u_{ik}^{NL} + F_{ik} \delta u_{ik}^L]_{k\,=\,i,j} = 0\end{aligned} \quad (2)$$

In Eq. (2), the superscripts '*L*', '*NL*', and '*o*', stand for linear, nonlinear, and equilibrium reference state quantities, respectively. There are only two none vanishing Green's strain components, and have the following linear and nonlinear terms;

$$\begin{aligned}e_{xx} &= u_c' - v_s''(y - z\phi) - w_s''(z + y\phi) - \omega\phi'' \\ &+ \frac{1}{2}\left[(v_s')^2 + (w_s')^2\right] + (z_s v_s' - y_s w_s')\phi' \\ &+ \frac{1}{2}\left[(z - z_s)^2 + (y - y_s)^2\right](\phi')^2\end{aligned} \quad (3a)$$

Of the two stress terms appearing in Eq. (2), the reference

$$e_{xx} = \frac{1}{2}\Theta\phi' \quad (3b)$$

equilibrium state stress component can be estimated from;

$$\sigma_{xx}^o = \left[\frac{N^o}{A}\right] + \left[\frac{M_y^o}{I_{yy}}\right] y + \left[\frac{M_z^o}{I_{zz}}\right] z + \left[\frac{M_\omega^o}{I_{\omega\omega}}\right] \omega$$

The other stress term, which is the incremental linear stress term σ_{ij}^{L} is determined from the corresponding linear strain components, which constitute the first five terms of Eq. (3a), by making use of appropriate constitutive relations. The remaining terms of Eq. (2) are the linear and nonlinear displacement terms and can be approximated from Eq. (1) by using, for convenience, the Taylor's series expansions of the trigonometric terms.

After substituting into Eq. (2) all the relevant quantities, and through variational treatment of the results, one obtains the following governing differential (equilibrium) equations;

$$EAu_c'' = p_x \tag{5a}$$

$$EI_{yy}v_s^{(4)} - N^o v_s'' + (-z_s N^o + M_z^o)\phi'' = p_y \tag{5b}$$

$$EI_{zz}w_s^{(4)} - N^o w_s'' + (y_s N^o - M_y^o)\phi'' = p_z \tag{5c}$$

$$EI_{\omega\omega}\phi^{(4)} - GJ\phi'' + (-z_s N^o + M_z^o)v_s'' + (y_s N^o - M_y^o)w_s''$$
$$- (r_s^2 N^o + \beta_y M_y^o + \beta_z M_z^o + \beta_\omega M_\omega^o)\phi''$$
$$+ [p_y^o(y_p - y_s) + p_z^o(z_p - z_s)]\phi = c_T \tag{5d}$$

Further, the associated boundary conditions at $x = 0$ and $x = L$ ($k = i$ and $k = j$) are;

$$u_c = u_{ck}$$
$$\text{or} \quad n_x[\,EAu_c'\,] = F_{xk} \tag{6a}$$

$$v_s = v_{sk}$$
$$\text{or} \quad n_x[-EI_{yy}v_s''' + N^o v_s' + (z_s N^o - M_z^o)\phi'] = F_{yk} \tag{6b}$$

$$-v_s' = -v_{sk}'$$
$$\text{or} \quad n_x[-EI_{yy}v_s'' - M_z^o\phi] = D_{yk} \tag{6c}$$

$$w_s = w_{sk}$$
$$\text{or} \quad n_x[-EI_{zz}w_s''' + N^o w_s' + (-y_s N^o + M_y^o)\phi'] = F_{zk} \tag{6d}$$

$$-w_s' = -w_{sk}'$$
$$\text{or} \quad n_x[-EI_{zz}w_s'' + M_y^o] = D_{zk} \tag{6e}$$

$$\phi = \phi_k$$
$$\text{or} \quad n_x[-(EI_{\omega\omega}\phi''' - GJ\phi') + z_s N^o v_s' - y_s N^o w_s'$$
$$+ (r_s^2 N^o + \beta_y M_y^o + \beta_z M_z^o + \beta_\omega M_\omega^o)\phi'$$
$$+ \{F_{yk}^o(y_p - y_s) + F_{zk}^o(z_p - z_s)\}\phi_k] = C_{Tk} \tag{6f}$$

$$-\phi' = -\phi_k'$$
$$\text{or} \quad n_x[-EI_{\omega\omega}\phi'']\,C_{\omega k} \tag{6g}$$

In Eq. (6), $n_x = -1$ at $x = 0$, and $n_x = 1$ at $x = L$.

The cross-sectional constants such as the moments of inertia that appear in the above two sets of equations have been defined in the preceding works[4,5]. However, the following other such quantities deserve special attention, due to the fact that differences in the symmetry conditions of the cross-sections are taken care of hy them;

$$\beta_y = -2y_s + \left(\frac{1}{I_{yy}}\right)\int_A [y\,(y^2 + z^2)]\,dA \tag{7a}$$

$$\beta_z = -2z_s + \left(\frac{1}{I_{zz}}\right)\int_A [z\,(y^2 + z^2)]\,dA \tag{7b}$$

$$\beta_\omega = \left(\frac{1}{I_{\omega\omega}}\right)\int_A [\omega\,(y^2 + z^2)]\,dA \tag{7c}$$

The above differential equations are important from a theoretical point of view and for obtaining analytical solutions. However, for general loading and boundary conditions these equations are difficult to solve, making it necessary to device some discrete computational procedure, employing some form of stiffness equations. Such a procedure has been described in Ref.[5], following the finite element scheme and making use of the well known Hermite interpolating polynomials, which produce the (14 times 14) stiffness equation given as;

$$\begin{Bmatrix} F_x + F_{ox} \\ F_y + F_{oy} \\ F_z + F_{oz} \\ T + T_o \end{Bmatrix} = \begin{bmatrix} K_{11} & & & sym. \\ 0 & K_{22} & & \\ 0 & 0 & K_{33} & \\ 0 & K_{42} & K_{43} & (K_{44} + K_a + K_b) \end{bmatrix} \begin{Bmatrix} U \\ V \\ W \\ \Phi \end{Bmatrix} \tag{8}$$

The block matrices K_{ij} $(i,j = 1,4)$, and the special matrices K_a and K_b that take care of the additional effects of load-point locations, are all given in Ref.[5]. Further, the computational procedure employing the above formulation uses efficient transformation and updating procedures.

The Linearized Formulation

The linearized method uses a reduced stiffness matrix that is extracted from the stiffness matrix of the general formulation. Only those terms that correspond to lateral and torsional degrees of freedom are taken, and the formulation is used to plot the linearized load-lateral and load-torsional displacement

curves. It has, in addition, been used to estimate ultimate strengths of members [2].

The theoretical background as well as the solution strategy for this linearized formulation has been adequately discussed in Ref. (2). In the solution strategy used for the linearized method, it was necessary to use the relations between changes in the stress resultants and the corresponding lateral and torsional displacements. For this reduced formulation, only two out of the four general governing differential equations given by Eq. (5) in the preceding section, that is, only Eq. (5b) and Eq. (5d), are relevant. Similarly, out of the seven general boundary conditions only four, that is, Eq. (6b), Eq. (6c), Eq. (6f), and Eq. (6g) are usable. It is strongly noted that, all incremental external load terms, which are the incremental distributed load terms in the governing differential equations as well as the incremental nodal force terms in the boundary conditions, do not appear in the differential equations defining for this linearized formulation.

The stiffness equation that was used for the linearized formulation, can symbolically be represented as;

$$\mathbf{f}' = \mathbf{K}_r\mathbf{d} = (\mathbf{K}_r' + \lambda_i\mathbf{K}_r^g)\mathbf{d} \qquad (9)$$

The reduced stiffness matrix $\mathbf{K}_r$ can be extracted from the stiffness matrix developed for the general formulation: while the elastic component $\mathbf{K}_r'$ can be taken out at any stage of loading, the stress or geometric component $\mathbf{K}_r^g$ must be extracted from the geometric component of the general stiffness matrix, after determining the latter for the unit value of the specified load.

The vector $\mathbf{f}'$ in Eq. (9) is an equivalent nodal load vector that replaces the nodal lateral and torsional imperfections. These elemental imperfections are transformed to elemental nodal forces through multiplication by the elemental elastic component matrix of the general elemental stiffness matrix. Therefore, since once defined the imperfections do not change, the equivalent nodal forces are constant quantities. If the beams are assumed to be perfectly free of such imperfections, then the problem represented by Eq. (9) reduces to an eigenvalue problem which has been used for the determination of lateral-torsional buckling loads.

It is not unrealistic to assume that most practical beams are initially geometrically imperfect. It is a common practice to model such imperfections by simple and common functions, trigonometric functions being the most widely used ones. Therefore, for simple beams pinned at both ends, the imperfections are represented by half-sine waves, and can be expressed as follows;

$$v_{sk} = v_o \sin\left(\frac{\pi x_k}{L}\right) \qquad (10a)$$

$$\phi_k = \phi_o \sin\left(\frac{\pi x_k}{L}\right) \qquad (10b)$$

Similarly, for cantilever beams, the imperfections are modeled by quarter-waves which can be expressed as;

$$v_{sk} = v_o \left[1 - \cos\left(\frac{\pi x_k}{2L}\right)\right] \qquad (11a)$$

$$\phi_k = \phi_o \left[1 - \cos\left(\frac{\pi x_k}{2L}\right)\right] \qquad (11b)$$

In the above of equations, 'v_o' and 'ϕ_o', are, respectively, the lateral and torsional imperfection amplitudes over the span lengths of the beams, and are correlated to each other by the following expression;

$$\phi_o = \frac{v_o}{h} \qquad (12)$$

The rates of changes of the lateral and torsional imperfections, v_{sk}' and ϕ_k', for both cases, are determined by the first derivatives of the corresponding functions.

At any stage of computation, the load level is changed by effecting the corresponding alteration on the load factor λ_i in Eq. (9). This can be done because the geometric component of the stiffness matrix is a linear function of the stress resultants. This means that the displacement components in the

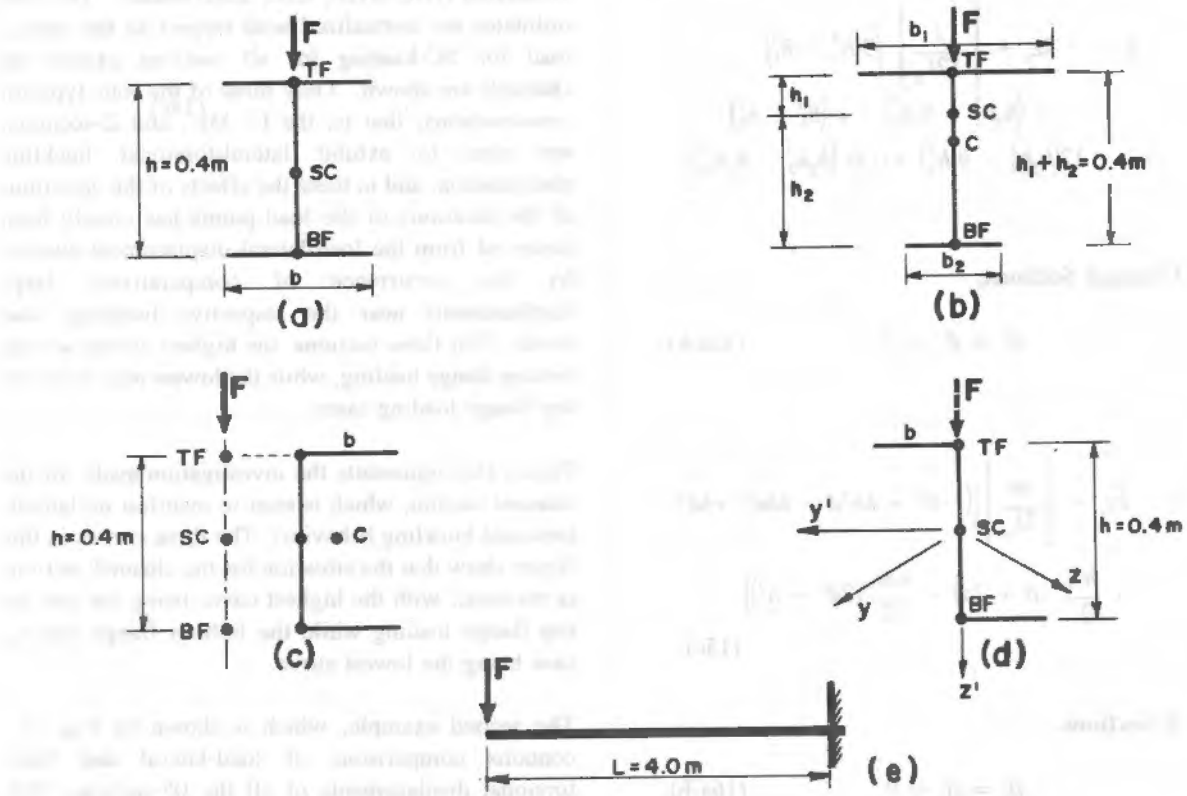

Figure 3 Selected Cross-Sections, and Locations of Load-Points

Selection of Cross-Sectional and Geometrical Details

vector **d** are total rather than incremental. After the assemblage of the reduced stiffness matrix and the equivalent load vector, then the displacement vector can be calculated.

Figure 3 shows four most common and simple cross-sections, representing the four different types of possible cross-sectional symmetry conditions. These are, the doubly-symmetric I-section shown in Fig. (3a), the mono-symmetric I-section which has a vertical axis of symmetry as shown in Fig. (3b), the channel section with a vertical web (having a horizontal axis of symmetry) shown in Fig. (3c), and dthe none-symmetric Z-section shown in Fig. (3d). For each type, three sizes of sections that differ in flange width have been selected. Therefore, for the oubly-symmetric I-shape, the channel shape and for the Z-shape, respectively, the I05, C05, and Z05-sections have a breadth b = 0.05m, the I10, C10, and Z10- sections have b = 0.10m, and the I15, C15, and Z15-sections have a breadth b = 0.15m. For the mono-symmetric I-sbape, the top and bottom flange widths differ, and are, respectively, for the MI05-section b_1 = 0.70m and b_2 = 0.30m, for the MI10-section b_1 = 0.12m and b_2 = 0.08m, and for the MI15-section b_1 = 0.17m and b_2 = 0.13m. Otherwise, all selected cross-sections have an identical depth of d = 0.40m, and same uniform thickness of t = 0.01m.

The tbree cross-sectional constants that were represented by Eq. (7), are determined using the following explicit equations for the four cross-section types:

(a) Doubly-Symmetric I-Sections;

$$\beta_y = \beta_z = \beta_\omega = 0 \qquad \text{(13a-c)}$$

(b) Mono-Symmetric I-Sections;

$$\beta_y = \beta_\omega = 0 \qquad \text{(14a-b)}$$

$$\beta_z = -2z_s + \left[\frac{t}{12I_{zz}}\right]\left[3\left(h_2^4 - h_1^4\right) + \left(h_2 b_2^3 - h_1 b_1^3\right) + t\left(b_2^3 - b_1^3\right) + 12\left(b_2 h_2^3 - b_1 h_1^3\right) + 18t\left(b_2 h_2^2 - b_1 h_1^2\right)\right] \quad (14c)$$

(c) Channel Sections;

$$\beta_z = \beta_\omega = 0 \quad (15a\text{-}b)$$

$$\beta_y = -2y_s + \left[\frac{bt}{2I_{yy}}\right]\left[\left(-b^3 + 4b^2 d - 6bd^2 + 4d^3\right) + \frac{h^2}{2}\left(-b + 2d\right) + \frac{hdt}{12}\left(12d^2 + h^2\right)\right] \quad (15c)$$

(d) Z-Sections.

$$\beta_y = \beta_z = 0 \quad (16a\text{-}b)$$

$$\beta_\omega = \frac{b^2 ht}{24(2b + h)I_{\omega\omega}}\left[4b^3 + 6b^2 h + 2h^3\right] \quad (16c)$$

Care was taken in the selection of the load-points, which are shown by the strong dots in Fig. (3), together with the identifications *SC*, *BF*, and *TF*, for shear center, bottom flange, and top flange, respectively. In every case, the original loads are assumed to be applied along the vertical axes containing the shear center of the respective cross-section, so as to prevent induced torsional loading. Fig. (3) shows the longitudinal arrangement of the cantilever beams which are used in the investigations.

NUMERICAL EXAMPLES AND DISCUSSIONS OF RESULTS

The Nonlinear Method

This method had been applied in the previous works [4,5] to trace load-displacement curves for beams having either doubly-symmetric or mono-symmetric I-sections. In the first example which is illustrated by Fig. (4), the effects of the variations of the locations of the load-points along the vertical axes containing the shear center is investigated using the 10-section (I10, MI10, C10, Z10) beams. The load ordinates are normalized with respect to the critical load for SC-loading for all sections except the channels are shown. Only three of the four types of cross-sections, that is, the I-, MI-, and Z-sections, are seen to exhibit lateral-torsional buckling phenomenon, and in these the effects of the variations of the locations of the load-points has clearly been observed from the load-lateral displacement curves, by the occurrence of comparatively large displacements near the respective buckling load levels. For these sections, the highest curves are the bottom flange loading, while the lowest ones were for top flange loading cases.

Figure (4c) represents the investigation made for the channel section, which is seen to manifest no lateral-torsional buckling behavior. The three curves in this figure show that the situation for the channel sections is reversed, with the highest curve being the one for top flange loading while the bottom flange loading case being the lowest curve.

The second example, which is shown by Fig. (5), contains comparisons of load-lateral and load-torsional displacements of all the 05-sections (I05, MI05, C05, and Z05). Bottom-flange loading was selected in the comparisons. As seen on Fig. (5a), which compares load-lateral displacement results, the largest lateral displacements occur for the I05 beam. The lateral displacements for the C05 section are seen to be extremely small. In Fig. (5b), the load-torsional displacement curves have been compared. The loads in both figures have been normalized with respect to the critical load for the I-section beam.

In the final example of this section, which is represented by Fig. (6), the relationships between flange width to web height ratio and the magnitude of lateral displacement has been investigated for all four cross-sections using SC-loading. The behaviors of the three types of sections that exhibit instability is again similar, with the largest maximum displacements occurring for the 05-sections while the smallest ones were for the 15-sections.

As before, the behavior of the channel section which is presented on Fig. (6c), is seen to be opposite to that of the other sections, with the largest lateral displacement being that of the C15-sections, and the

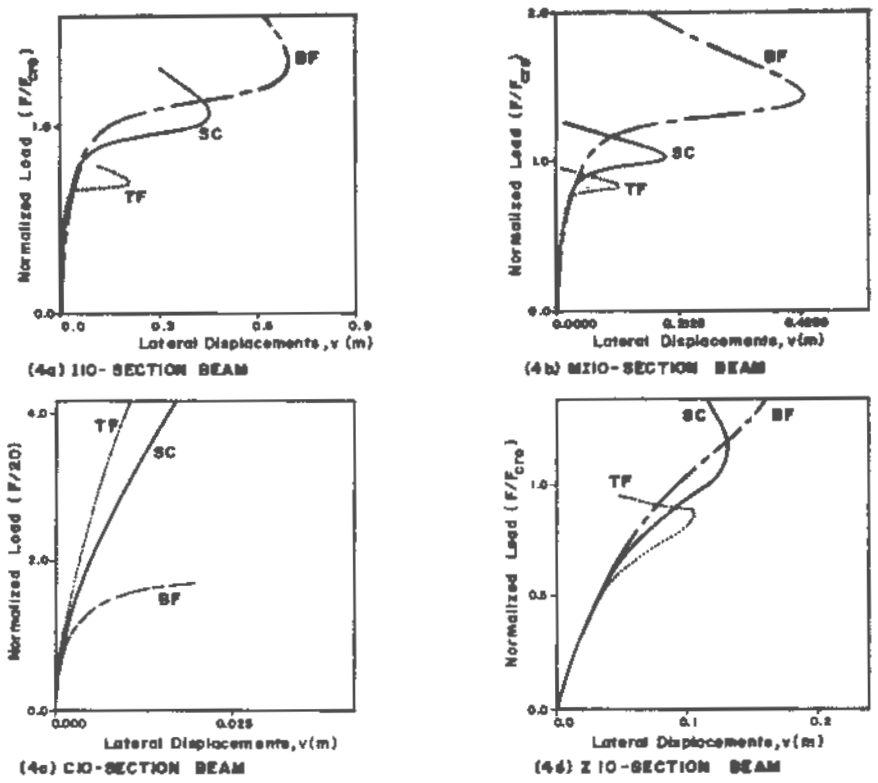

Figure 4: Effects of Load-point Location On the Load-Displacement Behaviour

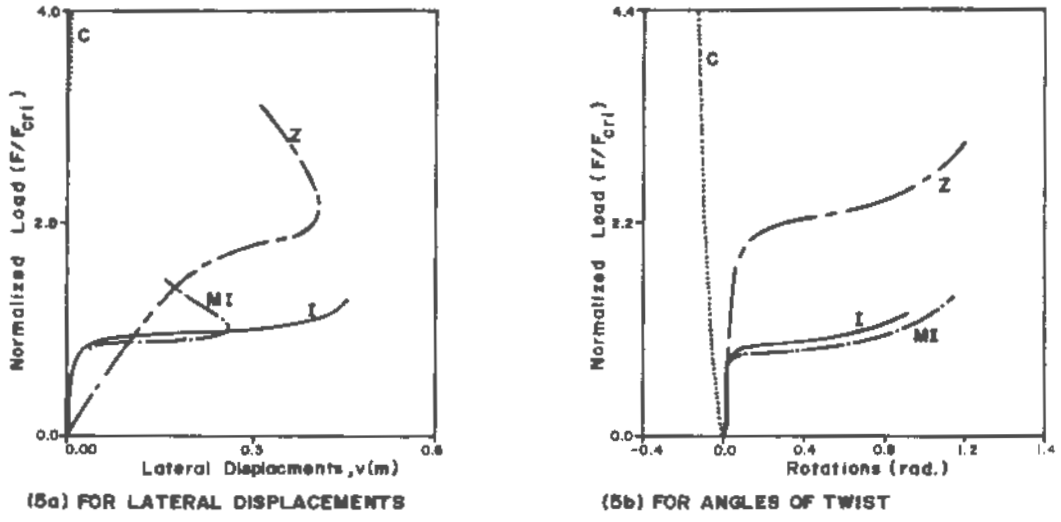

Figure 5: Comparison of Rotations and Lateral Displacements for 10SC Beams

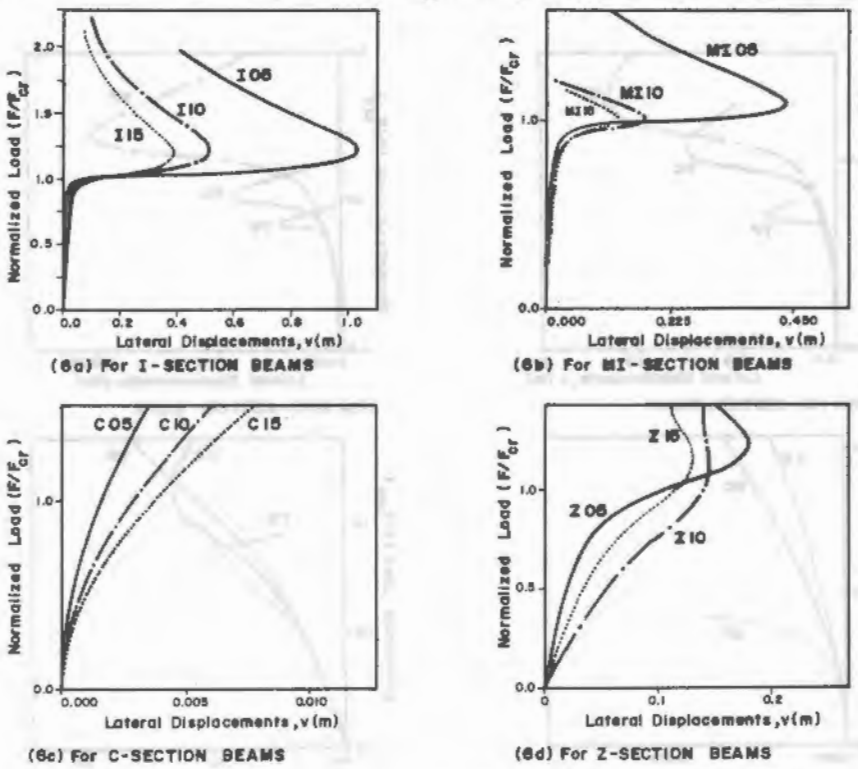

Figure 6 Effects of Flange Width on Load-Displacement Curves

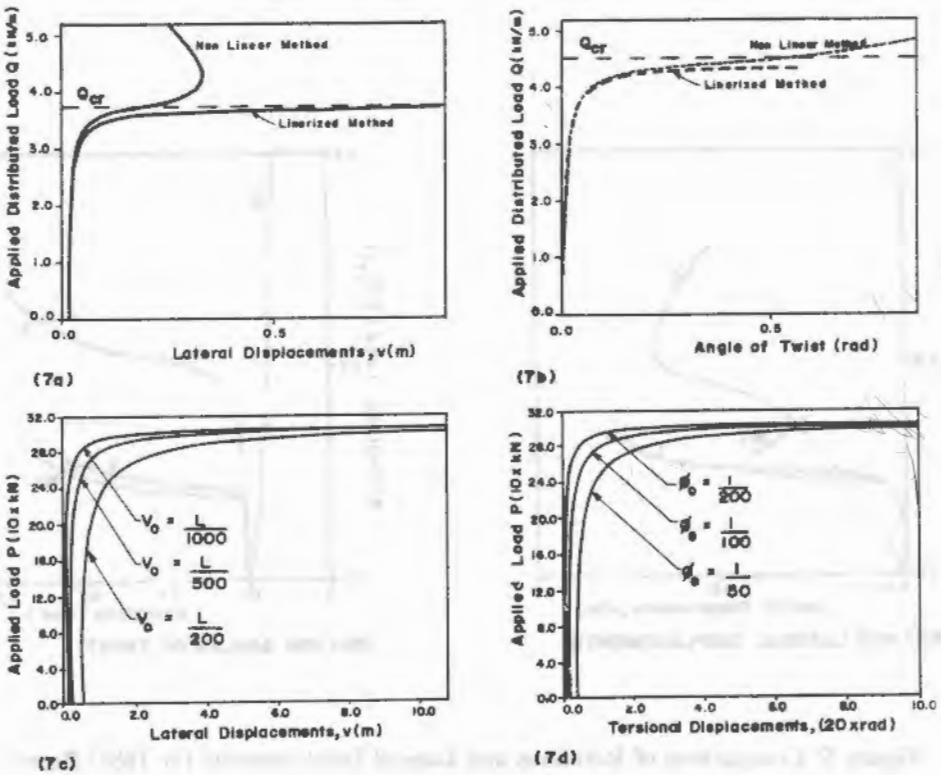

Figure 7 Accuracy and Important Characteristics of the Linearized Method

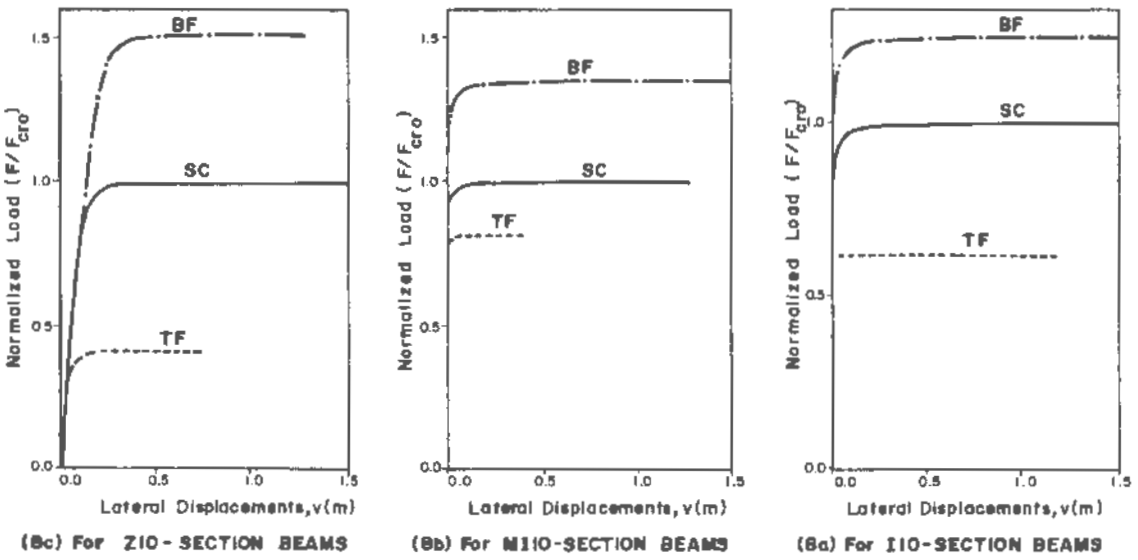

Figure 8 Effects of Load-Point Locations

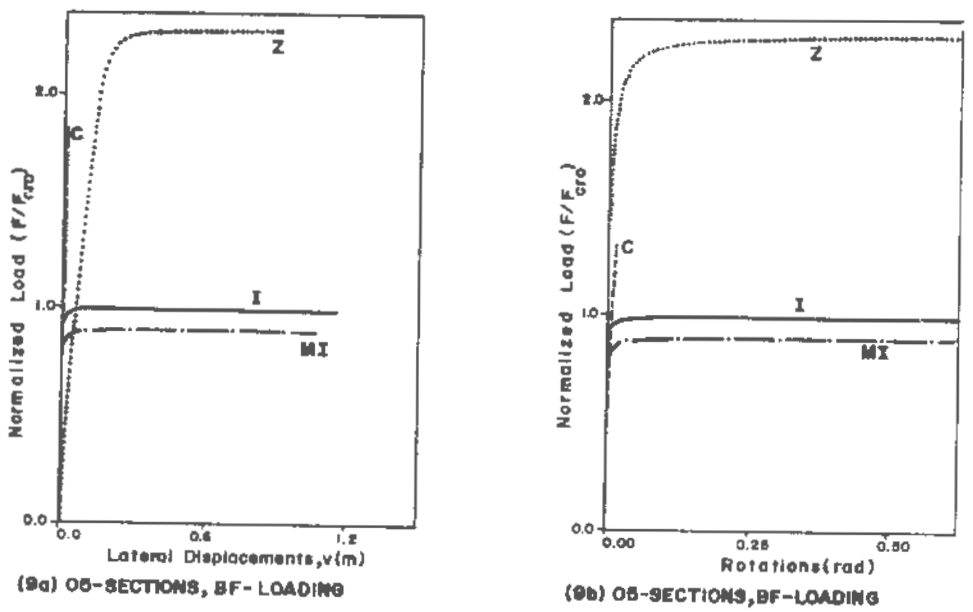

Figure 9 Comparison of Displacements

smallest one for the C05 beam. In Fig. (6), the loading have been normalized with respect to the buckling loads for every case.

The Linearized Method

As discussed previously[2], the linearized method is a linearization of the general nonlinear method. The basic characteristics of the linearized method which makes it different from the nonlinear method is that it avoids coordinate transformation, and updating of coordinate. In addition, the linearized method has only 8-degrees of freedom per element, as opposed to the 14-degrees of freedom for the nonlinear one. This was due to the fact that the linearized method considered lateral and torsional degrees of freedom only.

The first example in this section is reserved to the comparison of the linearized method with the nonlinear method so as to check the relative accuracy of the former, and to the illustration of its other unique characteristics, which are connected to the magnitude and nature of initial imperfections. In Fig. (7a), load-lateral displacement curves, for a simply-supported beam under top flange distributed loading, that have been drawn using the two methods, are compared. In Fig. (7b), for the same beam with the exception of the distributed load being applied at the shear center, the load-torsional displacement curves have been traced. In both cases, initial lateral imperfections only have been applied. These two comparisons show the excellent agreement between the two methods up to levels very near to the respective buckling loads.

Figures (7c) and (d) are devoted to the investigation of the effects of application of different magnitudes of the two types of initial imperfections: lateral or torsional imperfections. It is seen, for both cases, that the lowest curves correspond to the numerically largest imperfections, while the highest curves were for the smallest ones. However, in either case, all curves converge to the same critical load levels. These latter two investigations assure us of the possibility of modelling any form of geometrical nonlinearity using such initial imperfections with the linearized method.

The remaining two examples of this section deal with the same type of investigations as the first two examples, which were for the nonlinear method. Thus, in Fig. (8) the effects of the variations of the locations of the load-point were investigated for the three sections which exhibit lateral-torsional buckling phenomenon. In the last example, the load-lateral and load-torsional displacement curves were drawn, in Fig. (9a) and (b) respectively, and the same comparisons as in the second example of the preceding section were performed. These two last examples have shown that, the linearized method can be employed to give useful results as were obtained using the nonlinear method.

CONCLUSIONS

The applications of the theoretical development that was based on the finite displacement theory has been extended to the treatment of members having cross-sections that were not included in previous studies [4,5]. The development has been presented in forms of governing differential equations and stiffness equations, and the factors in them which take care of the effects of cross-sectional symmetry conditions have been explicitly and efficiently determined. A generalized nonlinear method has been employed to investigate the nonlinear pre-buckling as well as the post-buckling load-displacement behaviors of doubly-symmetric I-section, mono-symmetric I-section, channel section, and Z-section beams. Another reduced formulation, the linearized method has been used to study the pre-buckling load-displacement behaviors of the same members. The buckling loads were determined through eigenproblem solution scheme, which uses the stiffness matrix of the reduced linearized formulation. The following conclusions were made from observations of the computational results of the several illustrative examples presented in this study.

(a) While some previous researchers believed that both the channel section and Z-section beams did not exhibit lateral-torsional buckling, the present study has ascertained that this was true only for the channel section beams: both the load-displacement behavior studies using the two methods as well as the eigenproblem solution scheme have indicated that the Z-section beams manifest some form of lateral-torsional instability.

(b) The load-point location was seen to greatly affect not only the buckling loads (when there are any), but also the finite displacement behavior of all beams used in the study. For the channel sections which did not exhibit instability, the level of the curves was in reverse order.

(c) The channel and Z-section beams seem to show large reserve strengths as observed from their load-displacement curves, which were seen to be the highest during comparisons to those of the other sections. However, this has to be checked through some form of an ultimate strength study of the members, since this reserve strength also seems to correspond to fairly large stresses.

(d) The flange width to web height ratio has a definite effect on the load-displacement behaviors of all the members. While the response pattern for the sections that exhibit instability was similar, that for the channel section is seen to occur in reverse order, similar to what was seen in (b), above. This fact was the same for load-displacements studies using the nonlinear as well as the linearized method.

REFERENCES

(1) **Fukumoto, Y. and Kuho, M.,** "A Survey of Tests on Lateral Buckling of Beams," in the Preliminary Report of the Second International Colloquium on Stability, ECCS, Leige, April, 1977.

(2) **Dellelegne Teshome,** "A Simplified Ultimate Strength Estimation of Common Thin-Walled Cross-Section Beams with Lateral Loads Applied at Arbitrary Points." Proceedings of the Second International Conference on Structural Engineering Analysis and Modelling, SEAM 2 July 17-19, 1990, Kumasi, Ghana, pp. 257-266.

(3) **Hill, H. N.,** "Lateral Buckling of Channel and Zee Beams," Transactions of ASCE, Vol. 119, Paper No. 2700, pp. 829-841, 1956.

(4) **Dellelegne Teshome and Negussie Tebedge,** "Influence of Position of Load Application on the Behavior of Thin-Walled Members,"African Journal of Science and Technology, ANSTI, Vol. 7, No. 2, Oct. 1988, pp. 11-21.

(5) **Dellelegne Teshome**, "Effects of Points of Load Application on the Lateral-Torsional Buckling, Load-Displacement Behavior, and Ultimate Strength of Thin-Walled Members," Ph.D Dissertation, University of Tokyo, Tokyo, Japan, 1987.

(6) **Vlasov, V. Z.,** "Thin-Walled Elastic Beams," Israeli Programme for Scientific Translations, Jerusalem, 1961.

(7) **Barsoum, R. S., and Gallagher, R. H.**, "Finite Element Analysis of Torsional and Torsional-Flexural Stability Problems," International Journal of Numerical Methods in Engg., Vol. 2, pp. 335-352, 1980.

(8) **Bazant Z. P., and El Nimeiri, M.,** "Large Deformations Spatial Buckling of Thin-Walled Beams and Frames,"Journal of the Engineering Mechanics Division, ASCE, Vol. 99, No. EM6, Dec. 1973.

(9) **Zamost, G., and Johnston, E. R.,** "Post-Lateral Buckling Behaviour of Beams," Journal of the Engineering Mechanics Division, ASCE, Vol. 97, No. EM4, Aug. 1971.

(10) **Woolcook, S. T., and Trahair, N. S.,** "Post-Buckling Behaviour of Determinate Beams," Journal of the Engineering Mechanics Division, ASCE, Vol. 100, No. EM2, Apr. 1974.